Morphology and Adsorbate Dependence of Ionic Transport in Dye Sensitized Mesoporous TiO_2 Films

N. Papageorgiou,* C. Barbé, and M. Grätzel

Laboratory for Photonics and Interfaces, Swiss Federal Institute of Technology, CH-1015 Lausanne, Switzerland

Received: January 20, 1998; In Final Form: March 16, 1998

By modeling the steady-state mass transport in a thin-layer cell configuration involving an electrochemically inactive mesoporous colloidal film, the limiting currents of an iodine containing electrolyte can be predicted, as a function of the film porosity. The porosity of the layer is then determined by best fit of the porosity parameter in the model, given the experimentally determined limiting currents. Satisfactory agreement is found with the porosity values obtained by BET measurements. In photoelectrochemical cell applications such as dye sensitized nanocrystalline photoelectrodes for solar energy conversion devices, the porosities of the dye loaded films of e.g. anatase TiO_2 play an essential role with respect to their efficiency. In particular, the findings of this work demonstrate that the presence of adsorbed sensitizer *cis*-$(SCN^-)_2$ bis(2,2′-bipyridyl-4,4′-dicarboxylate)ruthenium(II) in TiO_2 colloidal films appears to decrease the original naked film porosity by up to 30%. This depends on the initial bare film porosity and the dye diameter, thus resulting in a considerably lower effective mass-transport limit within the coated films. The effective diffusion coefficient of triiodide in these porous electrodes was found to not deviate significantly with respect to the free-stream values, suggesting an influence of mesoporosity on the transport mechanisms involved.

Introduction

Porous structures, by virtue of the surface area enhancement that they offer, find many applications of technological and commercial interest. This has been the case with the development of efficient solar energy conversion devices based on porous semiconducting membranes, i.e., nanocrystalline TiO_2 films sensitized by suitable dyes.[1−3]

As currently fabricated, these structures have relatively narrow pore and particle size distributions, with values centered in the *meso*-domain i.e., the 2−50 nm range.[4] With a structure resembling the random packing of solid spheres of similar size, a controlled microporosity is expected. The effective ionic diffusion through the porous films is expected to be controlled essentially by the porosity and by a tortuosity factor. That is to say that the mass-transport properties within these films possibly result from a combined effect of the nanometer particle size and the type of packing, the degree of connectivity of the pore network—whether a structure does not allow for blind pores, diffusional loops, or cylindrical pore formation of multidirectional character, i.e., the nonoriented structure, etc. (see Results and Discussion). The possibility of expressing these features in terms of volume averaged parameters such as porosity and tortuosity make them especially suitable for mass-transport simulations, as they greatly simplify the modeling assumptions, through the low-scale macrohomogeneity of the medium, and lead to a higher definition model.

While the decrease of particle size in dye sensitized photoelectrodes may increase the total exposed surface area of semiconducting material to the electrolyte, the accessibility of the whole surface to the light sensitizing dye molecule for surface adsorption should be retained throughout the pore network. Moreover, the operation of a complete photoelectrochemical (PEC) device strongly depends on the dye regenerating function of the redox mediator contained in the electrolyte, which can only be conveyed via the porous network containing the electrolyte. The influence of photoelectrode porosity on solar cell performance, together with a comprehensive analysis of the mass transport in nanocrystalline film PECs has been reported elsewhere.[5,6] Given the porosity, the adsorbed dye concentration in the porous layer, and the total cell thickness, among other parameters such as diffusion coefficients of the ionic species, one can proceed in order to optimize the redox mediator operation, which in the case of the iodide/triiodide couple, consists of the minimization of photon absorbing triiodide and of the iodide concentration required in the electrolyte for efficient counter electrode operation and for efficient dye regeneration, respectively. Porosity, obviously, plays a significant role in the optimization of the PEC device. Models for the mass transport of iodide and triiodide at steady-state operation of a nanocrystalline solar cell indicate the tendency for triiodide accumulation at the photoelectrode and even more accute depletion of iodide in the same region. It was proved critical that in order to sustain efficient electron injection and charge collection at the photoelectrode, a certain iodide level should be maintained in the vicinity of each dye molecule.[7] Porosity appears as a decisive parameter with respect to the transport properties of all designs for nanocrystalline solar energy conversion devices known to date.[6,7]

In this work, a partly experimental method has been developed by which one can monitor the effectiveness of ionic transport inside bare and the same dye coated nanocrystalline films and explore the correlation between diffusion coefficient, porosity, or pore size distribution and the size of the sensitizer molecule, in both of the above cases. In conjunction with structural information from BET measurements, this principally

* To whom correspondence should be addressed. E-mail: nicholas.pappas@icp.dc.epfl.ch.

S1089-5647(98)00819-0 CCC: $15.00
Published on Web 04/30/1998

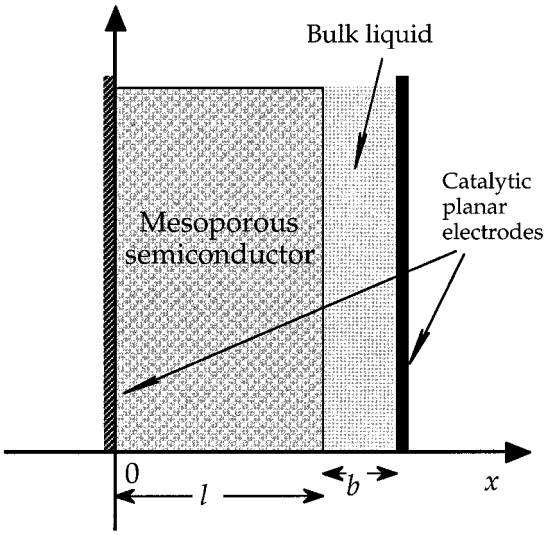

Figure 1. Schematic representation of an asymmetric thin-layer cell consisting of a mesoporous inert phase and a bulk liquid between two planar electrodes. Electrochemical reaction is confined to the planar electrodes, and current can flow in both directions.

electrochemical method relies on a simulation model describing the steady-state behavior of a redox relay couple in a thin-layer cell configuration that, furthermore, predicts the limiting currents attainable as a function of the cell characteristics and the electrolyte properties. When the experimentally determined limiting current values are incorporated into the simulation model, the mathematical fitting is achieved by adjustment of the porosity, i.e., the equivalent void volume available for electrolyte transport or, alternately, the effective diffusion coefficient in the cell.

Theoretical Model

The concentration profiles of a relay redox couple, e.g., iodide/triiodide, in a thin-layer cell comprising an electrode with a porous layer coupled with a regenerating planar catalytic counter electrode, are affected by the porosity and the separation between the porous anode and the planar counter electrode, on one hand, and generally on the ionic diffusivities of the electrolyte species, on the other.

In the interest of experimentally determining the effect of sensitizer adsorption on the effective relay function of the mediator, we have developed a steady-state theoretical mass-transfer model for a planar electrode cell with an inert and insulating colloidal film deposited on the one electrode and, in the general case, with space following the film up to the counter electrode. The model cell is schematically represented in Figure 1. The electrochemical reactions, and thus charge transfer, are confined to the planar electrode surfaces, the colloidal layer considered electrochemically inert. This should be distinguished from an alternative mode for the electron transfer, where reaction can take place on the planar conducting surface as well as on the porous layer surface of a current collector electrode, the porous layer thus considered electrochemically active as well as conducting, either via surface or bulk. Counter electrode reaction is always taken to be confined to the planar surface of the catalytic counter electrode. The oxidized form, I_3^-, and the reduced, I^-, of the redox mediator will henceforth be denoted as O and R, respectively.

To take into account the mesoporous nature of the colloidal film component of the cell, it is imperative to note that

$$C_{i,\text{liquid}} = C_{i,\text{av}}/\text{porosity} \qquad \text{(i)}$$

when the concentrations of species O and R within the porous phase are calculated, where $C_{i,\text{av}}$ is defined as the number of moles per unit volume of the porous cell space and porosity as the ratio of the void volume to total volume of the porous material. Considering the nanocrystalline layer as macrohomogeneous from a scale above the order of the colloidal particle diameter, it is possible to express all equations for the quasi-liquid system, using the $C_{i,\text{av}}$ values for concentrations and then by substituting from expression i, to get a general system of differential equations and boundary conditions (1−6), describing the steady state, using only liquid concentrations. An equivalent approach is to incorporate the porosity with the diffusion coefficient, defining thus an effective (volume averaged) diffusion coefficient $D_{i,\text{eff}} = D_i$ (porosity), assuming in this case that D_i (in the liquid) is influenced by the presence of the solid phase by way of film porosity, which is examined in Results and Discussion.

The subscripts O and R are used to denote quantities relevant to the I_3^- (oxidant) or I^- (reductant) species, respectively. The mesoporous semiconductor is characterized by a porosity, ϵ_p, the ratio of the volume of its pores to its total geometric volume. The following quantities are relevant to the proposed description: $C_{O,p}(x)$, $C_{R,p}(x)$ refer to the number of moles of the respective species per unit volume of liquid in the pores at position x. $C_{O,b}(x)$, $C_{R,b}(x)$ refer to the respective number of moles per unit volume of liquid bulk at position x. The symbols D_O, D_R denote the diffusion coefficients of the respective species in the liquid.

In the cell (see Figure 1), the porous material extends in the x-direction up to the point where the bulk layer begins and, of course, has no electrical contact with the cathode. The consumption of the reduced species, I^-, for the production of the oxidized species, I_3^-, must be compensated for by an equivalent conversion (reduction) back to iodide on the counter electrode, according to the reaction

$$I_3^- + 2e \leftrightarrow 3I^- \qquad \text{(ii)}$$

and inversely when the other case of oxidation occurring on the counter electrode is considered.

Ion diffusion occurs in the liquid. In the two-electrode thin-layer cell the reactions take place only on the planar electrode surfaces of the anode and cathode, where species R are oxidized and O are reduced. In such a situation, Fick's second law of diffusion must apply for both O and R at steady state (constant current passed). Taking into account the stoichiometry of reaction ii and ignoring ion migration at this time, the concentrations of the redox ions in the liquid obey

$$\frac{d^2C_{O,p}(x)}{dx^2} = 0, \qquad \frac{d^2C_{R,p}(x)}{dx^2} = 0 \qquad (1)$$

after having formulated the equation for the averaged concentrations and substituted from i. The porosity of the porous material and the diffusion coefficient do not appear in the expression since the production rate of the electroactive species O, R in the whole domain is zero. At the left electrode of the cell (see Figure 1), the current results from the reverse of the redox reaction taking place on the right electrode, implying that the net flux of either the oxidized or reduced species depends on

the current flowing, with equivalent fluxes for each species on the two sides, thus providing the boundary conditions. As a boundary condition the current, I, correlation to the flux J_i of the species at $x = 0$ is taken, according to the stoichiometry of the reaction

$$\left[\frac{dC_{O,p}(x)}{dx}\right]_{x=0} = -I/(2FD_O\epsilon_p), \quad \left[\frac{dC_{R,p}(x)}{dx}\right]_{x=0} = 3I/(2FD_R\epsilon_p) \quad (2)$$

where F the faraday, which stems directly from the fact that $J_i = -D_i\, dC_{i,av}(x)/dx$, and then substituting from i.

We now examine the effect of a more realistic cell design which incorporates a layer of bulk liquid of thickness b, as represented in Figure 1. The considerations that lead to eqs 1 and 2 are still valid for the part of the cell which contains the porous material. In the portion of the cell that contains only bulk liquid, the oxidized and reduced species will transport similarly by diffusion. The concentration of the ions in the bulk solution obey

$$\frac{d^2C_{O,b}(x)}{dx^2} = 0, \quad \frac{d^2C_{R,b}(x)}{dx^2} = 0 \quad (3)$$

At $x = l$, the transition between the porous material and the bulk liquid, additional relations have to be taken into account. The concentrations of the oxidized species and of the reduced species are identical in the liquid contained in the pores and in the liquid bulk.

$$C_{O,p}(l) = C_{O,b}(l), \quad C_{R,p}(l) = C_{R,b}(l) \quad (4)$$

Moreover, the flux of each species is also the same in either medium at the boundary $x = l$, so that

$$\epsilon_p\left(\frac{dC_{O,p}(x)}{dx}\right)_{x=l} = \left(\frac{dC_{O,b}(x)}{dx}\right)_{x=l}, \quad \epsilon_p\left(\frac{dC_{R,p}(x)}{dx}\right)_{x=l} = \left(\frac{dC_{R,b}(x)}{dx}\right)_{x=l} \quad (5)$$

Finally, we take into account the conservation of mass applied for O and R species. During steady-state operation, the total amount of each species contained in the cell per unit area is conserved. The number of moles of each species contained in the liquid inside the cell, i.e., in the pores and bulk layer per unit area of cell is equal to the initial mole quantity of either species initially introduced into the electrolyte. This is stated by the following equations:

$$\left.\begin{aligned}\epsilon_P\int_0^l C_{O,p}(x)\,dx + \int_l^b C_{O,b}(x)\,dx &= \epsilon_P C_O{}^* l + C_O{}^* b\\ \epsilon_P\int_0^l C_{R,p}(x)\,dx + \int_l^b C_{R,b}(x)\,dx &= \epsilon_P C_R{}^* l + C_R{}^* b\end{aligned}\right\} \quad (6)$$

where $C_O{}^*$ and $C_R{}^*$ are the initial concentrations of these two species in the electrolyte solution.

With boundary conditions eqs 2, 4, and 5, and with eq 6 being taken into account, the unique analytical solution for the system of differential equations (1) and (3) giving the concentration profiles of both species within the cell as a function of steady-state current through the cell is derived

$$\left.\begin{aligned}C_{O,p}(x) &= C_O{}^* - \frac{Ix}{2FD_O\epsilon_p} + \frac{Il}{4FD_O}\left[\left(1 + \frac{2}{\epsilon_p}\frac{b}{l} + \left(\frac{b}{l}\right)^2\right)\Big/\left(\epsilon_p + \frac{b}{l}\right)\right]\\ C_{R,p}(x) &= C_R{}^* + \frac{3Ix}{2FD_R\epsilon_p} - \frac{3Il}{4FD_R}\left[\left(1 + \frac{2}{\epsilon_p}\frac{b}{l} + \left(\frac{b}{l}\right)^2\right)\Big/\left(\epsilon_p + \frac{b}{l}\right)\right]\end{aligned}\right\} 0 \le x \le l$$

and in the bulk liquid

$$\left.\begin{aligned}C_{O,b}(x) &= C_O{}^* - \frac{Ix}{2FD_O} + \frac{Il}{4FD_O}\times \left[\left(2\epsilon_p - 1 + 2\frac{b}{l} + \left(\frac{b}{l}\right)^2\right)\Big/\left(\epsilon_p + \frac{b}{l}\right)\right]\\ C_{R,b}(x) &= C_R{}^* + \frac{3Ix}{2FD_R} - \frac{3Il}{4FD_R}\times \left[\left(2\epsilon_p - 1 + 2\frac{b}{l} + \left(\frac{b}{l}\right)^2\right)\Big/\left(\epsilon_p + \frac{b}{l}\right)\right]\end{aligned}\right\} l \le x \le l + b \quad (7)$$

for which the solution when $b = 0$ reduces to

$$\left.\begin{aligned}C_{O,p}(x) &= C_O{}^* + \frac{I}{2F\epsilon_p D_O}\left(\frac{l}{2} - x\right)\\ C_{R,p}(x) &= C_R{}^* - \frac{3I}{2F\epsilon_p D_R}\left(\frac{l}{2} - x\right)\end{aligned}\right\} \quad (8)$$

Assuming that a large excess of I^- is present, the diffusion of I_3^- toward the cathode can become limiting. Equations 7 and 8 will allow us to find the maximum current density attainable, for which, the reduction of I_3^- occurs as fast as it can be supplied by diffusion to the cathode. Its concentration in the vicinity of the cathode is then zero. The expression for the limiting current density, I_{lim}, in the simple case where $b = 0$ is obtained by

$$C_{O,p}(l) = 0 \text{ (in eq 8)} \Rightarrow I_{lim} = 4\epsilon_p FD_O C_O{}^*/l \quad (9)$$

We can note that the limiting current density is proportional to the porosity, the diffusion coefficient of the oxidize species, and its initial concentration. It is however inversely proportional to the cell thickness.

The expression for the limiting current density, $I_{lim\ b}$, in the case of a bulk liquid layer is obtained by

$$C_{O,b}(l+b) = 0 \text{ (in eq 7)} \Rightarrow I_{lim\ b} = \frac{4\epsilon_p FD_O C_O{}^*}{l}\left[\left(1 + \frac{b}{l\epsilon_p}\right)\Big/\left(1 + 2\epsilon_p\frac{b}{l} + \left(\frac{b}{l}\right)^2\right)\right] = I_{lim}\left[\left(1 + \frac{b}{l\epsilon_p}\right)\Big/\left(1 + 2\epsilon_p\frac{b}{l} + \left(\frac{b}{l}\right)^2\right)\right] \quad (10)$$

When the current flows in the opposite direction, the limiting current $I'_{lim\ b}$ is different from $I_{lim\ b}$ when $b \neq 0$ and identical for both directions when $b = 0$, as evidenced by the comparison of formulas 10 and 11. We can see that the limiting currents

are generally influenced by the ratio b/l value contained in the modifying factor by which I_{lim} of eq 9 is multiplied.

$$C_{O,p}(0) = 0 \text{ (in eq 7)} \Rightarrow I'_{lim\ b} = -\frac{4\epsilon_p F D_O C_O^*}{l}\left[\left(1+\frac{b}{l\epsilon_p}\right)/\left(1+\frac{2}{\epsilon_p}\frac{b}{l}+\left(\frac{b}{l}\right)^2\right)\right] = -I_{lim}\left[\left(1+\frac{b}{l\epsilon_p}\right)/\left(1+\frac{2}{\epsilon_p}\frac{b}{l}+\left(\frac{b}{l}\right)^2\right)\right] \quad (11)$$

For a given b exists one set of limiting currents corresponding to the two current directions, which should both define one porosity value. The porosity values determined from each current direction should therefore be identical.

$$\epsilon_p = \frac{I_{lim\ b}(b^2+l^2) - 4FD_OC_O^*b}{4FD_OC_O^*l - 2lbI_{lim\ b}} \quad (12a)$$

$$\epsilon_p' = \frac{-I'_{lim\ b}(b^2+l^2) - 4FD_OC_O^*b}{8FD_OC_O^*l} \pm \frac{[-32FD_OC_O^*bl^2I'_{lim\ b} + (4FD_OC_O^*b + I'_{lim\ b}(b^2+l^2)^2)]^{1/2}}{8FD_OC_O^*l} \quad (12b)$$

It turns out that ϵ_p is always positive, while from the two possible solutions for ϵ_p' one of these porosity values is negative, thus leaving the positive one as the only acceptable solution.

Experimental Section

Electrode Preparation and Characterization. A typical synthesis of the TiO_2 nanoparticles can be described as follows. A 125 mL aliquot of titanium isopropoxide (97%, Aldrich) is added, by drops and at room temperature, to 750 mL of a 0.1 M nitric acid solution under vigorous stirring. A white precipitate is formed instantaneously. Immediately after the hydrolysis, the slurry is heated to 80 °C and stirred vigorously for 8 h in order to achieve the peptization (i.e., destruction of the agglomerates and redispersion into primary particles). The solution is then filtered on a glass frit to remove nonpeptized agglomerates. Water is added to the filtrate to adjust the final solid concentration to around 5% in weight.

The growth of these particles up to 10−25 nm is achieved under hydrothermal conditions in a titanium autoclave heated for 12 h between 200 and 250 °C depending on the desired particle size. Sedimentation takes place during the autoclaving, and the particles are redispersed using a titanium ultrasonic horn (400 W, 15 × 2 s pulses). After two sonications the colloidal suspension is introduced in a rotary evaporator and evaporated (35 °C, 30 mbar) to a final TiO_2 concentration of 11% in weight. To prevent cracking during film drying and thus render the synthesis of 10 μm thick sintered films possible, poly(ethylene glycol) (M_w = 20 000, Merck) is added in a proportion of 0−50% of the TiO_2 weight. The resulting paste is stored in a screw threaded capped glass bottle until deposition.

The TiO_2 paste is deposited using a simple doctor blade technique on Nippon sheet glass coated with a fluorine doped SnO_2 layer of 8−10 Ω sheet resistance. The resulting green layer is approximately 100 μm thick. The layer is dried in air at room temperature for 10 min followed by a 15 min treatment around 50 °C. The film is then heated to 450 °C at 20−50 deg/min and left at 450 °C for 30 min before cooling to room temperature.

The sensitizer molecule was the *cis*-$(SCN^-)_2$ bis(2,2′-bipyridyl-4,4′-dicarboxylate)ruthenium(II). The dye was adsorbed on the colloidal TiO_2 film by placing the freshly heated (400 °C in air) electrode in a dry ethanolic solution of the dye, once it had cooled to 70 °C, for 1 h. Spectral absorbance data and Langmuir adsorption isotherm studies performed in our laboratory have shown that a closely packed monolayer surface coverage is expected under these conditions for this dye molecule; i.e., dye aggregation is not occurring.

The electrode microstructure was characterized using high-resolution scanning electron microscopy (SEM) Hitachi S-900 field emission microscope. The electrode pore size distribution was studied using a Micromeretics ASAP 2010 nitrogen adsorption−desorption apparatus. The surface area was calculated using the BET equation, and the Barret−Johner−Halenda (BJH) treatment was applied to the isotherm in order to calculate the pore size distribution.[8] The BET evaluation report presented an error of 0.65%.

Electrochemical Technique and Instrumentation. The Autolab P20 potentiostat of Ecochemie was used for cyclic and linear sweep voltammetry. The techniques were employed on the asymmetric thin-layer cells, as illustrated in Figure 1. The experimental cells consisted of two conducting glass electrodes treated with a triiodide reduction catalyst formed by platinization according to a previously described method.[9] On the other electrode the colloidal TiO_2 film was deposited,[1] which was held at constant separation from the other electrode by thin Mylar (Dupont) sheet "wedges" put between the electrodes, while under clamp pressure. When the TiO_2 film presented local protrusions of a submicron scale, a cell without a spacer also proved satisfactory. The cell separation could vary between 8 and 20 μm, depending on the film and spacing, while the surface area was ca. 0.7−1 cm^2, determined accurately (±0.1 mm^2) under optical microscope with a reference scale. Precise determination of the porous TiO_2 film thickness, l, essential for the application of the model, as well as the dimensional characteristics of the thin-layer cell configuration, i.e., the total separation of the electroactive electrode surface planes $l + b$, were performed by the TENCOR Instruments *alpha-step 200* and/or a TESA, model *Tesadigit* high-precision digital micrometer to an uncertainty better than 5%.

The above two-electrode arrangement was gradually polarized at a rate, e.g., 100 mV/s, until a current plateau was reached and the limiting current resulting from the reduction of triiodide at the cathode could thus be measured. Consequently, one electrode was exposed to anodic and the other to cathodic conditions, and the polarity then reversed on the cell in order to measure the two limiting currents corresponding to the two current flow directions, as predicted by the model developed in the previous section.

A typical cell was filled with electrolyte containing 30 mM I_2 dissolved in a prepared mixture of 1-hexyl-3-methyl imidazolium iodide (MHImI) at a concentration of 900 mM, which corresponds to 18 wt %. The redox relay couple was contained in electrolytes comprising ambient temperature ionic liquids such as MHImI and ethylmethylimidazolium bistriflylimide ($MEIm^+Tf_2N^-$). The negligible volatility and the very wide electrochemical window assured the constancy of the triiodide concentration in the electrolyte and the hydrophobic character of $MEIm^+Tf_2N^-$ as solvent protected the redox couple from side reactions with atmospheric moisture. The synthesis of all molten salts employed herein has been described elsewhere.[10] To reduce the contribution of ionic migration to the diffusional flux of triiodide, pure molten salts were used as solvent and as

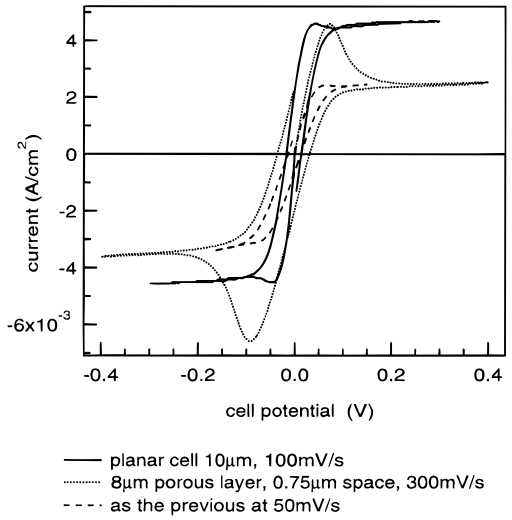

Figure 2. Experimental cyclic voltammograms depicting the limiting currents in both polarization modes. The electrolyte was 0.9 M MHImI 30 mM I_2 in MEImN$(CF_3SO_2)_2$.

an iodide source. The determination of triiodide diffusion coefficients in the particular choice of electrolytes for the experiment and under the same conditions was done using a thin-layer technique, described elsewhere in detail.[5]

The experimental cell was placed in a dark-box while experiments were carried out, to avoid the generation of photoconductivity in the semiconductor, which therefore behaved as an insulating separator.

Results and Discussion

The experimental limiting current values recorded using the above electrolytes appear independent of the scan direction (scanning from zero polarization toward either positive or negative potentials) and of the sweep rate within the 50−400 mV/s range examined. At these scan rates a sharp leveling curve can be produced that has as plateau the limiting current in that direction, since edge migration of the electroactive species to/from the surrounding excess electrolyte cannot play a measurable role on the time scale of the experiment. Examples of experimental voltammograms depicting the limiting currents in both polarization modes can be seen in Figure 2. Note the current direction asymmetry in the case of a cell with a bulk layer resulting in two distinct limiting current values corresponding to each current flow direction. As expected, when the cell is geometrically symmetric, i.e., without a bulk electrolyte layer in the cell, then identical behavior in both polarization directions with respect to the two limiting currents is observed.

The ionic liquids utilized offer sufficient stability within the potential region employed, since their electrochemical window is extremely large.[10] With the catalyst treatment, the electrode SnO_2 substrates are made extremely active with respect to the iodide/triiodide reaction and could well have exchange currents around 200 mA/cm^2,[9] which results in a kinetic resistance of around 0.1 Ω·cm^2. This reduces the kinetic overpotential contribution, resulting in a sharper plateau formation.

The sensitizer coated TiO_2 colloidal film is theoretically electro-inactive at least up until its oxidation potential, i.e., 0.85 V vs SCE.[3] The planar electrode potential is thus removed from the I^-/I_3^- potential, i.e., approximately 0.15 V vs SCE, by only the concentration overpotential, therefore providing that the limiting current can be practically established within a cell polarization of around 250 mV. Also, the energetic distribution of acceptor states in the TiO_2 semiconductor is extremely small, at least up to 0.4 V vs SCE in both polarization directions,[11] and therefore capacitive currents from electrode differential capacity did not produce artifacts during the experiment, presenting a flat limiting current plateau in both directions as well as overlap of the forward and back scans within the limiting region (see Figure 2). It is noted that all experiments were conducted in the dark precisely in order to avoid electron injection and recapture between TiO_2 (bare or sensitizer coated) and the redox species, so that the relay electron transfers occur strictly on the planar current collectors—a prerequisite for the validity of the above proposed mathematical model.

The composition of the tested electrolytes ensures that triiodide is the current limiting species under the experimental conditions employed. First, because sufficient excess of I^- is provided, i.e., greater by 20 times the respective triiodide concentration, and second, because of the fact that $D_{I^-}/D_{I_3^-} = 1-1.3$ from the reported literature in dimethyl sulfoxide (DMSO), dimethylformamide (DMF), and AcN,[12,13] the condition $C_O D_O < {}^1/_3 C_R D_R$ can be satisfied,[14] thus ensuring a limitation by triiodide. Moreover, the electrode separation and therefore the thin-layer thickness δ (equivalent to the Nernst diffusion layer of semiinfinite diffusion) is of the order of ≈10 μm, and therefore well within the region $\delta < 200$ μm, where $I_{lim}\delta =$ constant.[14] That is to say that the limiting current is linearly related to the electrode separation because convection is negligible.

Ion migration of electroactive triiodide is expected to be minimal due to the presence of nonelectroactive supporting electrolyte in high concentration. In brief, the high ionic strength of the molten salt electrolyte minimizes the influence of the electric field, i.e., the migration of the charged triiodide species. Triiodide migration under the electric field between the electrodes is in the direction from cathode to anode and therefore opposes the diffusion process. This can be particularly important in cases such as solar cells where the migration tends in the direction opposite from the desired diffusional flux toward the counter electrode, and especially considering that triiodide is used in lower concentrations because of its absorption up to 500 nm.[6] It also follows that iodide migration adds to its diffusion in the cell but is of no consequence on the experiment. However, negligible ion migration of electroactive triiodide is expected under the above experimental conditions because of much higher iodide concentration and the presence of nonelectroactive molten ionic liquid as supporting electrolyte. For instance, in the case when molten salt is around 10 °/w, the sum of iodide and the spectator ion concentration results in a close to 1% influence on the triiodide limiting current and hence the same deviation in the diffusion coefficient determination.[6] The influence of the addition of a nonelectroactive ionic electrolyte on the limiting current of the triiodide ion cathodic reduction is seen in Figure 3, depicting behavior in a planar nonporous thin-layer cell as calculated from the model accounting for both diffusion and migration contributions.[6] A 5% decrease of the ideal-infinite conduction support limiting current where no migration is considered can be practically alleviated with the addition of a supporting electrolyte salt MX to 1 M in the system. Also, the calculated values for MI addition are identical to the ones shown in Figure 3. From the model it was therefore seen that the addition of 20% MHImI (around 1 M) suffices in rendering migration a negligible effect. Moreover, the experimental electrolyte composed of pure ionic liquids has a total concentration of the supporting ions of the order of 7−8 M, as back-calculated from their density, which is very

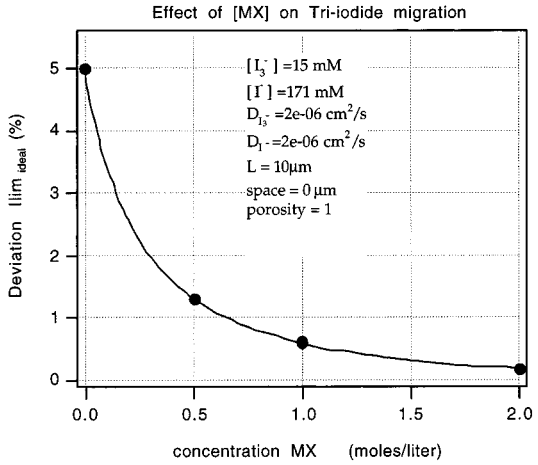

Figure 3. Plot indicating the deviation of the triiodide limiting current from pure diffusion as a result of ionic migration, as a funtion of supporting electrolyte content. Model results for a planar regenerative cell (see text).

high even if it is assumed that their activity is practically much lower due to extensive ion pairing. In fact, in this respect a conclusion can be drawn from the comparison of $\sigma\eta$ (the product of the specific conductivity and the dynamic viscosity) for neat molten salt and a dilute (0.5 M) in an organic solvent. As follows from the derivation of the product,[10] $\sigma\eta \approx yC$(constant), where C is the ionic concentration and $0 < y < 1$ is the dissociation fraction, which is justified for the same ions. By calculation of the product from the experimental data,[5] it appears that the dissociation fraction of the molten salt does not change significantly, at least not more than 10% with regard to the diluted systems.

With a total ion concentration of the order of 1 M of monovalent ions, the double layer thickness is <10 Å,[15] and therefore we can reasonably assume that under the present condition of much higher concentrations electroneutrality is achieved at any x-position in the liquid present in the pores. Moreover, double-layer effects should not be a concern in this study of dye coated films because, first, it is reduced to the order of several angstroms in the high ionic strength of the pure ionic liquid electrolyte employed, i.e., to a thickness not larger than the dye cross-sectional diameter (14 Å), and second, the dye coating the surface cannot be considered charged to form a compensating diffuse double layer extending beyond its diameter, due to the strong ligand screening, and since the electron density is mainly located on the attaching groups ($-COO^-$) close to the TiO_2 surface, through prevailing ester-like linkage.[16] However, in the case of a bare TiO_2 film in the presence of the electrolyte, the double layer of a few angstroms that is expected to establish at the interface can be accounted for, as will be shown below. It should be noted that as the neat films are left after heating at 400−450 °C to cool in ambient conditions, hydroxylation by chemisorption of water on coordinatively unsaturated surface Ti^{4+} ions occurs followed by proton transfer to a nearby O^{2-} ion, creating equal numbers of basic and acidic groups on the surface.[17] As net surface charge is therefore expected to be small, specific adsorption from solution species should minimally contribute to a structured double layer.

The pore size distribution of the TiO_2 thin film as measured from the BET technique is presented in Figure 4. The pore size is centered around 18.5−19 nm, and the distribution is quite narrow. The surface area is 126 m^2/g. If we assume that the particles are quasi-spherical, we can back-calculate an average

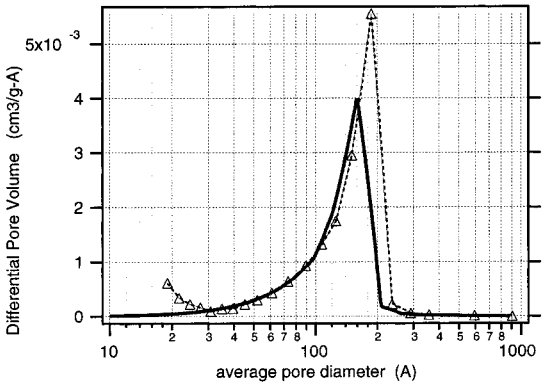

Figure 4. Pore size distribution of the nanocrystalline film prepared as described in the Experimental Section (△), compared to the calculated distribution in the case of the dye loaded film (solid line) when taking $D_{dye} = 1.4$ nm.

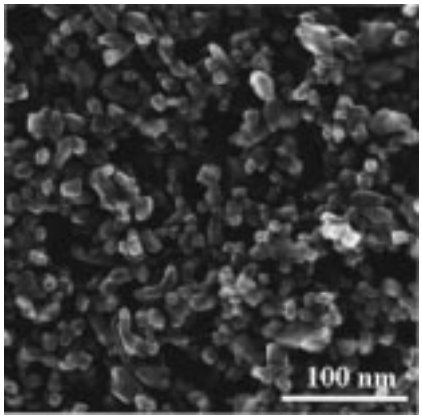

Figure 5. Micrograph by SEM of a typical nanocrystalline TiO_2 layer.

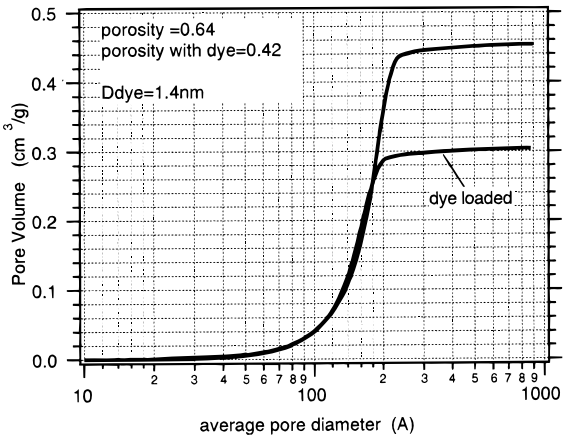

Figure 6. Cumulative pore volume as calculated from the pore size distribution of the nanocrystalline film in Figure 5.

particle diameter of 15 nm. This particle size is confirmed by scanning electron microscopy (see Figure 5).

The cumulative pore volume is shown in Figure 6, which depicts the comparison between the BET data for the naked TiO_2 film and that calculated on the basis of a pore diameter reduction of $2D_{dye}$ due to coverage of the sensitizer molecule onto the surface of the solid structure. In the case of the above-described nanocrystalline preparation, the cumulative pore volume values, derived from the measured N_2 adsorption (BET), reached a plateau of 0.456 cm^3/g (error < 1%). Given the density of anatase TiO_2, 3.85 g/cm^3, the porosity is given by V_{pore}/V_{total}, i.e., $0.456/(0.456 + {}^1/_{3.85}) = 0.640 \pm 0.005$. Thus, the nanocrystalline film is 64% porous. The porosity for the

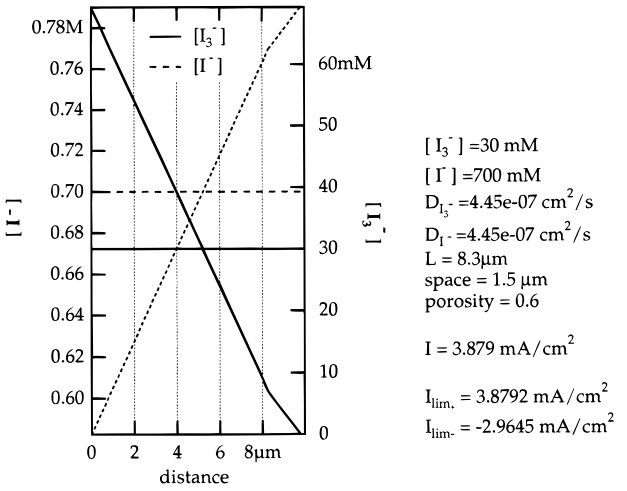

Figure 7. Concentration profiles of iodide and the triiodide ions at the steady-state limiting current, as well as at zero current, i.e., initial conditions (horizontal lines). The parameters reflect the actual geometric conditions of the experimental cell and the electrolyte properties. Depicted is the situation of one current direction, i.e., triiodide limited at the counter electrode side.

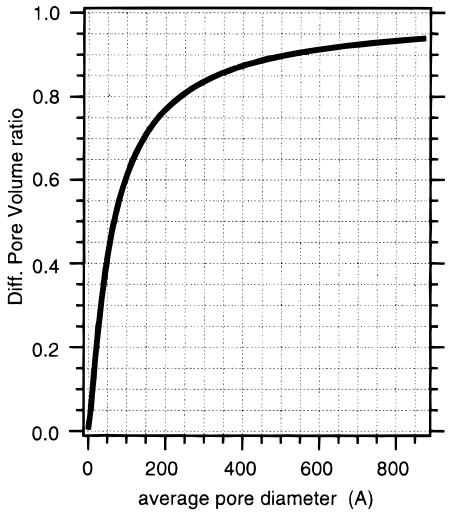

Figure 8. Differential pore volume ratio calculated for a spherical pore shape approximation and an adsorbed dye diameter of $D_{dye} = 1.4$ nm.

neat films was reproducibly found to be 0.60 ± 0.01 with the fit to the model of the experimental limiting currents. A typical model fitting result is depicted in Figure 7, displaying graphically the predicted concentration profiles of the iodide and triiodide in the case of current limitation on the bulk side electrode. Note that there is a discrepancy between the experimental and the calculated data. A viable explanation can be offered by the assumption of a small double layer present (e.g., 0.3−0.4 nm) covering the entire solid/electrolyte interface that would be calculated as a shift in the pore size distribution, and which according to the same as the above calculation results in a 0.59−0.60 film porosity. This explains to a good approximation the above difference in values between the electrochemical and BET methods.

After dye deposition the porosity as determined through the experiment−model method was 0.40 ± 0.01. The cumulative volume as derived from the modified distribution by dye adsorption, taking $D_{dye} = 1.4$ nm[18,19] (Figure 4) provides a porosity value of $0.302/(0.456 + {}^{1}/_{3.85}) = 0.422 \pm 0.005$. The lower porosity may indeed reflect the total blocking with respect to triiodide diffusion of the smaller sized pores, i.e., of the order of the dye diameter.

The differential pore volume ratio shown in Figure 8 indicates the measure of the volummetric change resulting from dye adsorption, which displays a strong dependency on the initial pore size. The tendency for change of the pore volume with the variation of the pore diameter can be expressed by the derivative of the volume with respect to the diameter value: $dV/dD = N(D)^{1}/_{6}\pi[(D + dD)^3 - D^3]/dD$, when assuming the approximations of a quasi-spherical pore shape, and $N(D)$ is the pore size distribution. By substituting D for $D - 2D_{dye}$ in the above, the expression for the dye coated film is formed. The differential pore volume ratio is thus defined as

$$dV_{dye}/dV = [(D - 2D_{dye} + dD)^3 - (D - 2D_{dye})^3]/[(D + dD)^3 - D^3]$$

which depends only on the magnitude of D_{dye}. From Figure 8 it is observed that, for a given D_{dye}, it would be desirable to have a pore size distribution centered at higher values, as this would imply that the dye deposition influences to a lesser degree the porosity of the film.

Since the triiodide diffusion coefficient in the liquid that was input as the model parameter was taken to be identical in magnitude to the one measured by the independent method described previously,[5] the close coincidence of film porosity values found by both methods represents a situation where the diffusion in the liquid phase does not change, within the estimated 5% experimental error, in the presence of the solid colloidal matrix. The relative to the particle size magnitude of the mean jump distance of triiodide in the liquid (<1 nm)[20], in addition to the inherent structural characteristics of the film, i.e., full pore connectivity and the lack of cylindrical pores (nonoriented porous solid)—a fact intimately dependent on the size and the shape and stacking mode of the particles, could be responsible for this behavior. Conversely, it is apparent that platelet shaped particles of larger size would influence the root-mean-square displacement, as the diffusional path for an ion would be larger in order to circumvent the larger surface projection normal to the net movement direction. For gas diffusion, with jump distances larger than the film particles, obstruction to the transport occurs from collision.[20] Certainly, the very low degree of microporosity as a result of a surface formed by random packing of distinct quasi-spherical particles, as well as the larger scale agglomerates comprising the solid phase, also allows for less obstruction to diffusive transport.

Generally, the concept of effective diffusivity is used to correct for the phenomena modifying the diffusion in porous media. Effective diffusivity accounts for the fact that (i) not all area normal to the direction of flow is available (i.e., void) for the molecules or ions to diffuse, (ii) the paths are tortuous, and (iii) the pores are of varying cross-sectional areas. This is usually expressed as $D_{eff} = D\epsilon_p/\tau$, where D is the free-stream diffusion coefficient and τ the tortuosity factor.[21] The above expression implies that besides the porosity the value of τ, a correction factor pertaining to the pore geometry, length, and orientation, should generally influence the diffusivity through a porous medium. In fact, the tortuousity factor is also defined as $\tau = TS$, where T is the tortuosity due to the increased path length and S the constriction factor which takes into account the special effects due to the convergent−divergent nature of the capillaries, i.e., the variation in the cross-sectional area that is normal to diffusion. Note that generally $T \geq 1$ and $S \geq 1$, with unity corresponding to pores parallel to the direction of macroscopic flow and to pores of uniform diameter, respectively. According to the definition of tortuosity,[21] in the case of a

spherical object between two points in the direction of net flow (circular path), a value of $T = 1.5$ is calculated. For the dense random packing of hard spheres, a fully connected porous network, $\tau = 1.44$.[22] A loose random pore structure gives $\tau = 1.7$, and a random pore model, $\tau = 3$.[23] A theoretical estimate of the tortuosity when all pore directions in a volume are assumed to be equally probably gives a value of 2, independent of pore radius.[24] Also for randomly oriented straight lines as pores, and for a cubic network built up from the same repeating element, the value is 3.[25] As is apparent from the evidence shown above, the tortuosity of the TiO_2 films examined is unlikely to be smaller than the minimum case value of, e.g., $\tau = 1.44$. Accepting this minimum value for the film tortuosity, the modulation on the D_{eff} would result ≈31% reduction of its value and in a fitted porosity of ≈0.42 by the experimental technique as compared to the 0.61 found. Therefore, the surprisingly small deviation observed for the D_{eff} in the presence of the solid phase from its free-stream value demonstrated in the experimental results raises the question on the mechanism of transport in these mesoporous films.

In proposing a speculative explanation for the unimpaired diffusion of triiodide through this porous network, one could consider that the nanometer particle/pore dimensions are stimulating a spherical diffusion process, which should become operative locally when conditions are within a scale simulating the ultramicroelectrode (normally from the micrometer range down). For spherical diffusion, the rates of mass transport increase rapidly with the decreasing size of the ultramicroelectrode (UME), for which the mass-transfer coefficient is of the order of D/r, where D is the diffusion coefficient and r the UME radius.[26] Therefore, complementary mass transport by spherical diffusion should be compensating for the local structural obstruction to the ionic movement due to the coexisting solid with the liquid phase, given the nanometer scale of these local concentration depletion phenomena.

One can create a notion of the "mesoscopic" diffusion mechanism by taking a cross-section of the porous medium and examining the mass transfer from a volume differential containing a constant concentration toward the adjacent cross-sectional plane normal to the net diffusive flow. At this plane the concentration is assumed to be, e.g., zero, in the limiting case, providing the concentration gradient driving force for transport. Given the quasi-spherical character of the particles comprising the porous layer and the anisotropy (nonoriented) with respect to the structure, from the cross-sectional areas belonging to the pores, where diffusion is possible, there would be on average over a larger surface compared to the particle dimensions, a distribution of two types of pore areas. On the one side there would be a percentage of pores that extend as openings into the selected volume, creating a funnel effect simulating the fundumental mass-transfer process of the UME, and thus enhanced transport under the concentration gradient established. For this type, diffusion layer overlap is restricted by the pore walls. The other end of the distribution concerns pores with constrictions resulting from the extension of the pore cross-section becoming narrower. Transport to the cross-sectional plane is now impeded through local diminution of the concentration gradient. For random pores, the fractional areas of both types of pore configurations on the cross-section plane are equal and therefore the two transport modes should closely counterbalance each other. The effective diffusion coefficient would be determined by the ratio of surface holes/total area, which, for random pores using Dupuit's law, is equivalent to the internal void fraction;[23] i.e., with regard to the average mass transport the modification from the free-steam diffusion value is accounted for by the porosity as the correction factor. Under the experimental conditions employed and the type of film structures produced, the tortuosity impediment to the diffusion appears to be counteracted by the operation of the more effective than planar, spherical diffusive mode, which is especially effective under steady state.[27−30] This mechanism is further enhanced by the many defects in the packing that create a primary and secondary porosity, as observed by SEM, and allows multiple paths around the constrictions inhibiting local transport.

Several theoretical analyses have appeared in the literature, formulating the general mass-transport problem.[31] It has not been, however, possible to test the agreement with the equations for transport in porous electrodes as applied to our experimental layers due to the complexity and the many unknown parameters required to represent the real system. From a first approach, it is apparent that the volume averaging technique evoked for the analysis, would not, for example, account for the nanometer scale localized gradients and the consequent stimulation of spherical diffusion involved in the overall mass transport, as of its very need to average over sufficiently large volumes.

It has been shown that triiodide transport is increased by a contribution of ion-hopping to the diffusion as iodide concentration is increased. This increase, however, as expressed by the variation in the Einstein−Stokes ratio, appears to amount to less than 10% relative to the diluted values at the iodide levels of the experimental electrolyte, as derived from previous mass transport studies in these systems.[5,10] Moreover, the overall transport mechanism would be the same whether in free stream or in the biporous system, and therefore the tortuosity should in principle have the same influence on the mobility of triiodide in the situation involving hopping and without. In conclusion, the argument of ion-hopping contribution to the transport mechanism on the basis of these data on transport in molten salt systems is insufficient for explaining the deviation of at least 31% from the expected D_{eff} values.

Additionally, there was no indication that a variation of iodine concentration in the test electrolyte had a measurable influence on the derived porosity value from the limiting current−transport model correlation, suggesting that iodine or triiodide adsorption onto the solid porous layer did not occur to an extent that altered the effective transport properties of triiodide. The search for an optimum triiodide concentration in the test electrolyte was based on the advantages arising from temperature control of the experimental cell at larger time scales, i.e., slower sweep rates, as too high a limiting current passed can generate sufficient heat from inherent electrolyte resistivity to possibly change the viscosity of the medium.

The above evidence suggests that the effective diffusion coefficient in these films is influenced predominately by the porosity, whereas tortuosity apparently assumes a minor role in the transport. Concerning the comparison between the mass transport of triiodide in the naked and the dye loaded film, the effective diffusion coefficient in the dye loaded film is decreased by approximately one-third relative to the same bare TiO_2 film. This decrease we have attributed to a commensurate decrease in the film porosity from the dye deposited on its surface, as the same decrease in porosity (within 5% uncertainty) has been calculated starting from purely geometrical considerations of void occupation in the pore walls by the dye, quantified finally as an alteration in the pore size distribution.

The BET measurements of internal surface area and porosity were not considered suitable in the case of the dye loaded films, as the adsorption of N_2 would not be restricted to the outer

surface of the dye interface due to its small volume, and therefore not be an objective measure of the void volume available for triiodide transport.

Conclusion

By means of a mass-transfer model and the experimental limiting current data of a thin-layer cell, an electrochemical technique has been developed enabling the determination of the effective diffusion coefficients of triiodide in porous TiO_2 films, as well as in the same films after sensitizer molecule adsorption. The experimental evidence from this work has shown that the effective diffusivity is essentially controlled by the change in the porosity of the colloidal TiO_2 mesoporous films in the bare state and, when dye coated, as the pore size distribution and the void fraction in the solid can be modified with the adsorption of sensitizer molecules onto its surface. The decrease in the porosity relative to the bare colloidal film was shown to extend up to 30% its initial value on the above-described colloidal films when *cis*-$(SCN^-)_2$ bis(2,2′-bipyridyl-4,4′-dicarboxylate)ruthenium(II) is adsorbed, a result that is particularly important with respect to the performance and the design requirements of dye sensitized nanocrystalline solar cell devices. The assumption that the diffusion coefficients of iodide/triiodide in the liquid filling the pores are very little affected by the presence of the solid nanocrystalline TiO_2 structure contained in the cell other than by a porosity correction is substantiated by the agreement of the model prediction with the BET evaluation of the naked TiO_2 porosity.

Acknowledgment. One of the authors (N.P.) extends a special thanks to R. Humphrey-Baker for valuable suggestions on the presentation and the clarity of the text and to F. Lenzmann for discussion on the BET data. We are grateful for the financial support of this work by INAP (Institute for Applied Photovoltaics, Gelsenkirchen, Germany) and the European Community through the JOULE III program.

References and Notes

(1) O'Regan, B.; Grätzel, M. *Nature* **1991**, *353*, 737.

(2) Grätzel, M. *Coord. Chem. Rev.* **1991**, *111*, 167.

(3) Nazeeruddin, M. K.; Kay, A.; Rodicio, I.; Humphry-Baker, R.; Müller, E.; Liska, P.; Vlachopoulos, N.; Grätzel, M. *J. Am. Chem. Soc.* **1993**, *115*, 6382.

(4) Sequeira, C. A. C.; Hudson, M. J. *Multifunctional Mesoporous Inorganic Solids*; Mathematical and Physical Sciences, Vol. 400; Kluwer: Dordrecht, The Netherlands, 1993; p 4.

(5) Papageorgiou, N.; Athanassov, Y.; Armand, M.; Bonhôte, P.; Pettersson, H.; Azam, A.; Grätzel, M. *J. Electrochem. Soc.* **1996**, *143* (10), 3099−3108.

(6) Papageorgiou, N.; Grätzel, M.; P.Infelta, P. *Sol. Energy Mater. Sol. Cells* **1996**, *44*, 405−438.

(7) Papageorgiou, N.; Grätzel, M. Counter Electrode Design in Multilayer Nanocrystalline Photoelectrochemical Solar Cells. Submitted for publication in *Sol. Energy Mater. Sol. Cells.*

(8) Heimenz, P. C. *Principles of Colloid and Surface Chemistry*, 2nd ed.; Dekker: New York, 1986.

(9) Papageorgiou, N.; Maier, W. F.; Grätzel, M. *J. Electrochem. Soc.* **1997**, *144* (3), 876−884.

(10) Bonhôte, P.; Dias, A. P. Papageorgiou, N. Kalyanasundaram, K.; Grätzel, M. *Inorg. Chem.* **1996**, *35*, 1168.

(11) Kay, A.; Humphrey-Baker, R.; Grätzel, M. *J. Phys. Chem.* **1994**, *98*, 952−959.

(12) Arvia, A. J.; C.Giordano, M.; Podesta, J. J. *Electrochim. Acta*, **1969**, *14*, 389−403.

(13) *Encyclopedia of Electrochemistry of the Elements*; Bard, A., Ed.; Dekker: New York, 1973; p 139.

(14) Schmidt-Weinmar, H. G. *Ber. Bunsen-Ges.Phys. Chem.* **1967**, *71* (1), 91−101.

(15) Bard, A. J.; Faulkner, L. R. *Electrochemical Methods, Fundumentals and Applications*; Wiley: New York, 1980; pp 500−511.

(16) Murakoshi, K.; Kano, G.; Wada, Y.; Yanagida, S.; Miyazaki, H.; Matsumoto, M.; Murasawa, S. *J. Electroanal. Chem.* **1995**, *396*, 27−34. and references cited therein.

(17) Kay, A. Ph.D. Thesis, No 1214, Swiss Federal Institute of Technology, Lausanne, 1994.

(18) Shklover, V.; Nazeeruddin, M.-K.; Zakeeruddin, S. M.; Barbé, C.; Kay, A.; Haibach, T.; Steurer, W.; Hermann, R.; Nissen, H.-U.; Grätzel, M. *Chem. Mater.* **1997**, *9*, 430.

(19) Bolliger, B.; Hochstrasser, M.; Erbudak, M.; Nissen, H.-U.; Zakeeruddin, S. M.; Nazeeruddin, M.-K.; Grätzel, M. *J. Solid State Chem.*, in press.

(20) *Physical Chemistry*, 4th ed.; Atkins, P. W., Ed.; Oxford University Press: Oxford, U.K., 1990; pp 722−738, 761−773.

(21) Fogler, H. S. *Elements of Chemical Reaction Engineering*; Prentice Hall: Englewood Cliffs, NJ, 1992; p 608.

(22) Levitz, P. *J. Phys. Chem.* **1993**, *97*, 3813−3818.

(23) Froment, G. F.; Bischoff, K. B. *Chemical Reactor Analysis and Design*; Wiley: New York, 1976; pp 163−177 and 167.

(24) Chzmadzhev, Yu. A. Chirkov, Yu. G. *Porous Electrodes*; Comprehensive Treatise of Electrochemistry Vol. 6; Plenum Press: New York, 1983; Chapter 5, p 325.

(25) Dullien, F. A. L. *Porous Media: Fluid Transport and Pore Structure*; Academic Press: New York, 1979; Chapter 4, p 225.

(26) Bard, A. J. et al. The Electrode/Electrolyte Interface-A Status Report. *J. Phys. Chem.* **1993**, *97*, 7147−7173.

(27) Southampton Electrochemistry Group. *Instrumental Methods in Electrochemistry*; Horwood: Hemel Hempstead, U.K., 1985; p 48.

(28) Bard, A. J.; Faulkner, L. R. *Electrochemical Methods, Fundumentals and Applications*; Wiley: New York, 1980; p 145.

(29) Bockris, J. O'M.; Reddy, A. K. *Modern Electrochemistry*; Plenum Press: New York, 1970; Vol. 2, Chapter 10, p 1219.

(30) *Ultramicroelectrodes*; Fleischmann, M., Pons, S., Rolison, D. R. Schmidt, P. P., Eds.; Datatech Systems Inc.: 1987.

(31) De Vidts, P.; White, R. E. *J. Electrochem. Soc.* **1997**, *144* (4), 1343−1353, and references cited therein.